

Infrared predissociation spectra of $\text{Ne}_n\text{-HN}_2^+$ clusters ($n=1-5$)

Sergey A. Nizkorodov,^{a)} Markus Meuwly,^{b)} John P. Maier, and Otto Dopfer^{c)}
Institut für Physikalische Chemie, Universität Basel, Klingelbergstrasse 80, CH-4056, Switzerland

Evan J. Bieske
School of Chemistry, University of Melbourne, Parkville, 3052 Australia

(Received 29 January 1998; accepted 23 February 1998)

Infrared predissociation spectra of $\text{Ne}_n\text{-HN}_2^+$ ($n=1-5$) cluster ions have been recorded in the vicinity of the N–H stretching vibration (ν_1) of HN_2^+ . Several bands of the Ne-HN_2^+ dimer are rotationally resolved and provide direct information on the geometry, intermolecular stretching and bending frequencies, and complexation induced frequency shift of the ν_1 vibration. The Ne-HN_2^+ complex has a linear, proton bound structure with an average separation between the Ne atom and the HN_2^+ center-of-mass of $\langle 1/R^2 \rangle^{-1/2} = 3.28 \text{ \AA}$. The observed characteristics of the dimer are reproduced by a two-dimensional intermolecular potential energy surface calculated at the MP2 level, that is adiabatically corrected to account for the coupling of the intramolecular N–H stretching and intermolecular motions. The binding energy in the vibrational ground state of the complex is found to be 795 cm^{-1} and increases to 1005 cm^{-1} upon excitation of the N–H stretching vibration. Although the spectra of the larger complexes are not rotationally resolved, shifts in the ν_1 transition frequency suggest that the larger clusters possess structures where the Ne atoms are weakly attached to the side of a linear Ne-HN_2^+ core. © 1998 American Institute of Physics. [S0021-9606(98)00521-2]

I. INTRODUCTION

Proton bound complexes are the intermediates of proton transfer reactions, that are important in a broad range of chemical environments.¹⁻⁴ In order to better understand the nature of the reaction intermediates a series of infrared spectroscopic studies of simple dimer systems consisting of either a rare gas atom or H_2 molecule bound to HN_2^+ or HCO^+ has been undertaken.⁵⁻¹⁵ The spectra, which for the most part are rotationally resolved, give detailed information on the interaction between the contributing moieties and should eventually provide the basis for potential energy surfaces for ion-neutral interactions at close range. The subject of the current paper is the previously unreported Ne-HN_2^+ complex.

Spectroscopic studies¹⁶⁻¹⁸ show that proton bound dimers prefer configurations where the proton can be most effectively shared between the bonded ligands. For example, the complexes Rg-HCO^+ ($\text{Rg}=\text{He, Ne, Ar}$) (Refs. 6–8, 19) and Rg-HN_2^+ ($\text{Rg}=\text{He, Ar}$) (Refs. 5, 11, 14) are linear while $\text{H}_2\text{-HCO}^+$ and $\text{H}_2\text{-HN}_2^+$ are found to be T-shaped,^{12,13,15} structural conclusions that are supported by *ab initio* calculations.^{12,13,20-23} Thus, the complex between Ne and HN_2^+ can be anticipated to be linear with the rare gas atom attached to the proton end of HN_2^+ .

Because of the large disparity in the proton affinities of Ne (201 kJ/mol) and N_2 (495 kJ/mol),³ the Ne-HN_2^+ com-

plex can be viewed in first approximation as an HN_2^+ molecule weakly distorted by a Ne atom. However, the proton is expected to be attracted by the rare gas atom, with the extent of the transfer sensitively influencing the frequency of the N–H stretching vibration (ν_1). The range of this effect is illustrated by comparing the weakly bound He-HCO^+ complex,⁸ where the ν_1 vibration is lowered by mere 12.4 cm^{-1} , and the more strongly bound Ar-HN_2^+ complex, where the red shift is of the order of 1000 cm^{-1} .⁵ For the Rg-HCO^+ series ($\text{Rg}=\text{He, Ne, Ar}$), a linear correlation between the rare gas atom's proton affinity and the red shift of the C–H stretching vibration has been noted.⁶

To assist the understanding of the interactions in the Ne-HN_2^+ complex and the interpretation of its infrared spectrum, *ab initio* and rovibrational calculations have been carried out, with predictions of average bond distances, intramolecular and intermolecular vibrational frequencies, and dissociation energies. The method involves the construction of two-dimensional intermolecular potential energy surfaces (PESs) adiabatically corrected for the N–H stretch motion. These are subsequently used in rovibrational calculations to determine the properties of the complex with the HN_2^+ core in the ground and ν_1 vibrational states. As the model was developed and extensively tested for He-HN_2^+ ,¹⁰ comparison between the two complexes is possible.

In the current work spectra of larger $\text{Ne}_n\text{-HN}_2^+$ complexes containing up to five neon atoms have also been recorded. In an earlier study of HCO^+ clustered with up to 13 Ar atoms,⁷ geometries were inferred from the Ar atom induced shifts in the ν_1 transition frequency, combination band positions, band profiles, and photofragmentation yields. The data are in accord with structures where a linear proton

^{a)}Present address: JILA, University of Colorado, Boulder, Colorado 80309-0440.

^{b)}Present address: Department of Chemistry, University of Durham, Durham, DH1 3LE, England.

^{c)}Author to whom correspondence should be addressed.

bound Ar–HCO⁺ core ion is surrounded by less strongly bound Ar atoms. The ligands first fill two five-membered solvation rings around the linear dimer core, with the first solvation shell completed by the attachment of the twelfth Ar atom at the oxygen end. Because of unfavorable signal to noise ratio similar studies of the He_{*n*}–HN₂⁺ and Ne_{*n*}–HCO⁺ series were limited to *n* ≤ 2. Spectra of Ne_{*n*}–HN₂⁺ clusters with *n* ≤ 5 presented here provide an opportunity for more extensive comparison with the Ar_{*n*}–HCO⁺ series.

II. EXPERIMENT

The infrared (IR) photodissociation experiments on the Ne_{*n*}–HN₂⁺ clusters were conducted in a tandem mass spectrometer.^{7,12,24} The apparatus utilizes an ion source that combines a pulsed supersonic expansion with electron impact ionization. Ionization occurs close to the nozzle orifice (≤ 1 mm), allowing the ions to cool and participate in clustering reactions with the expanding atoms and molecules. From previous experience it is expected that most ions are cooled into the ground vibrational state with a rotational temperature of roughly 20–40 K.¹⁵ Following their extraction from the plasma, the ions are focused into a quadrupole mass filter tuned to transmit the desired species. After deflection through 90° by a quadrupole bender, the parent ion beam is injected into an octopole ion guide, where photodissociation takes place. Photofragment ions are transmitted by a second quadrupole mass filter and sensed by an ion detector. Photodissociation spectra are obtained by recording the HN₂⁺ fragment ion yield as a function of the IR frequency.

Three isotopic modifications of the Ne–HN₂⁺ complex were investigated. In addition to the most abundant isotopomer ²⁰Ne–¹H¹⁴N₂⁺ (hereafter called “normal”), selected transitions of the ²²Ne–¹H¹⁴N₂⁺ and ²⁰Ne–¹H¹⁵N₂⁺ complexes were also recorded. The ²⁰Ne–HN₂⁺ and ²²Ne–HN₂⁺ complexes were created using a mixture of N₂, H₂, He, and Ne (ratio 1:8:50:600) at 6–8 bar. The natural abundance of ²²Ne (≈ 10%) is sufficient for the formation of usable quantities of ²²Ne–HN₂⁺. To produce Ne–H¹⁵N₂⁺, a mixture containing ¹⁵N₂, H₂, and Ne was prepared with an initial ratio of 1:5:20. The reservoir was refilled with H₂ and Ne as the gas was consumed, so that the proportion of ¹⁵N₂ dropped over time until the Ne–H¹⁵N₂⁺ beam became too weak for practical purposes. Due to the cost of ¹⁵N₂ only a limited number of scans were recorded for Ne–H¹⁵N₂⁺ and consequently the precision for its rotational line wave numbers is somewhat lower than for the other two isotopomers. The spectral ranges covered for ²⁰Ne–H¹⁴N₂⁺, ²²Ne–H¹⁴N₂⁺, and ²⁰Ne–H¹⁵N₂⁺ are, respectively, 2700–3500 cm⁻¹, 3000–3250 cm⁻¹, and 2960–3140 cm⁻¹. For ²⁰Ne–H¹⁴N₂⁺ spectra were also recorded in the 2ν₁ region between 5740 cm⁻¹ and 6100 cm⁻¹. The larger complexes, ²⁰Ne_{*n*}–H¹⁴N₂⁺ (*n* = 2–5), were studied in the vicinity of the N–H stretching vibration (ν₁) between 3020 and 3130 cm⁻¹.

Tunable IR radiation was generated by a pulsed commercial OPO system (3–5 ns pulse width, 20 Hz) covering the 2500–6900 cm⁻¹ range with 0.02 cm⁻¹ resolution. The intensity of the IR beam, measured with an InSb photovol-

taic detector, was used for normalizing the photodissociation signal. A fraction of the laser beam was directed into an optoacoustic calibration cell containing OCS, HDO, or NH₃. The line positions of these reference gases²⁵ combined with étalon fringes from the OPO oscillator output were used for wavelength calibration of the photodissociation spectra. As the laser and ion beams counter propagate, a small Doppler correction was applied to the peak positions in the photodissociation spectra. For each rotationally resolved band 3–6 scans were recorded at a speed of ≈ 0.005 cm⁻¹/s. The spectra were calibrated independently and the line positions were averaged. Because of averaging, relative line positions are believed to be somewhat more accurate (≈ 0.01 cm⁻¹) than the specified laser resolution (0.02 cm⁻¹). The absolute precision is limited by the uncertainty in the translational energy of the ions in the octopole region (± 1 eV). A value of 0.02 cm⁻¹ provides a conservative upper limit.

III. THEORY

In this section the structure and energetics of the Ne–HN₂⁺ dimer are examined from a theoretical viewpoint. Comparison with He–HN₂⁺ (*D*₀ = 542 cm⁻¹) (Refs. 10, 11) and Ar–HN₂⁺ (*D*₀ = 2781 cm⁻¹) (Ref. 5) leads to the expectation of a Ne··HN₂⁺ binding energy of approximately 1000 cm⁻¹. Therefore, the experimental data, with measured intermolecular stretching (ν_s) and bending (ν_b) frequencies of the order of 100–150 cm⁻¹ (see below), provide information on the lower lying parts of the potential energy surface. In order to explore the Ne··HN₂⁺ interaction in regions that are not spectroscopically probed, adiabatically corrected *ab initio* intermolecular potentials were constructed with HN₂⁺ in both its ground and ν₁ vibrational states. The veracity of these two-dimensional surfaces near the potential minimum was tested by comparing measured and calculated average bond distances, vibrational band shifts, and intermolecular vibrational frequencies. The procedure has been described in detail for He–HN₂⁺ where theoretical predictions were made for average structures, dissociation energies, and vibrational frequencies.¹⁰

A. *Ab initio* geometry and harmonic frequencies

As a first step, an *ab initio* geometry optimization of Ne–HN₂⁺ was performed using the GAUSSIAN 94 program package.²⁶ The basis set consisted of V TZ Ahlrichs functions for the core electrons, augmented by diffuse and polarization atomic orbitals from the aug-cc-pVTZ basis set.²⁷ This composition of basis functions has been successfully employed for other proton bound ion-rare gas systems.^{10,21} The contraction scheme can be described by N(10s,6p,3d,2f) → [6s,3p,3d,2f], H(5s,3p,2d) → [3s,3p,2d], and Ne(11s,7p,3d,2f) → [7s,4p,3d,2f]. The geometry optimization resulted in a linear proton bound configuration with bond lengths of r_{NN} = 1.1053 Å, r_{NH} = 1.0421 Å, and r_{HNe} = 1.7044 Å (Table I). No other minimum was located. The optimization of the free HN₂⁺ ion at the same level of theory led to a linear equilibrium geometry with r_{NN} = 1.1050 Å and r_{NH} = 1.0307 Å, in good agreement with the experimental values (Table I). Complexation with Ne lengthens the N–H

TABLE I. *Ab initio* structures and harmonic frequencies for HN_2^+ and Ne-HN_2^+ . Available experimental values are given for comparison.

	r_{NN} (Å)	r_{NH} (Å)	R (Å)	ω_1 (cm ⁻¹)	ω_s (cm ⁻¹)	ω_b (cm ⁻¹)
HN_2^{+a}	1.0927	1.0337		3399		
HN_2^+ (expt)	1.0928 ^b	1.0336 ^b		3405 ^c		
HN_2^{+d}	1.1050	1.0307		3394		
Ne-HN_2^{+d}	1.1053	1.0421	3.2442	3203	160	113

^aReference 35.^bReference 44.^cReference 34.^dThis work.

bond by 0.011 Å, indicative of significant interaction between the Ne atom and the proton end of HN_2^+ . On the other hand the N–N bond is almost unaffected.

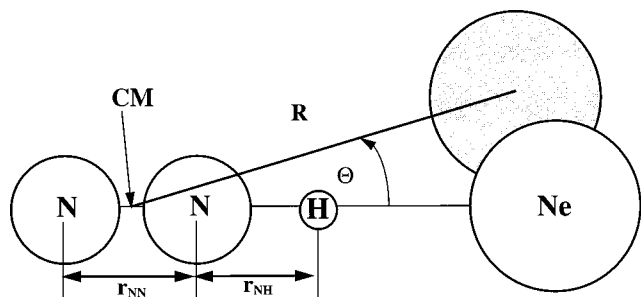
Using geometries found at the MP2 level, harmonic frequencies were calculated for both the free HN_2^+ monomer and the complex. Table I summarizes the vibrational data for HN_2^+ and Ne-HN_2^+ determined at the MP2 level and compares them with available literature values. In the harmonic approximation, the complexation induced red shift in ν_1 amounts to 191 cm⁻¹.

B. Rigid monomer PES

In order to further explore the $\text{Ne} \cdots \text{HN}_2^+$ interaction a two-dimensional intermolecular *ab initio* potential energy surface (PES) was constructed whereby the HN_2^+ was frozen in the optimized equilibrium geometry of the complex ($r_{\text{NN}} = 1.1053$ Å, $r_{\text{NH}} = 1.0421$ Å) while the Ne atom position was varied over a range of the Jacobi coordinates R and Θ (Fig. 1). This framework is referred to as the rigid monomer approximation, which assumes that the structural parameters of HN_2^+ are insensitive to the Ne atom's presence. The Boys and Bernardi scheme of counterpoise correction was employed to account for the effect of the basis set superposition error.²⁸ Interaction energies were calculated for 12 radial points along 13 different equally spaced angles Θ between 0° and 180°. The splined²⁹ rigid monomer PES, denoted as $V(R, \theta)$, is 896 cm⁻¹ deep with its minimum located at $R_e = 3.288$ Å in the linear proton bound configuration.

C. The adiabatic correction

The rigid monomer PES does not account for the interaction between the intermolecular and intramolecular mo-

FIG. 1. Coordinate system used to define the position of the neon atom with respect to the HN_2^+ ion.TABLE II. Coefficients a_i for the adiabatic correction function [Eq. (1)].

	a_1 (cm ⁻¹)	a_2 (a_0^{-1})	a_3	a_4 (a_0^{-1})
$v_1=0$	-62 476.0	1.039 7	96.029	0.477 12
$v_1=1$	-277 288.0	1.085 0	56.740	0.368 76

tions. Depending upon its position, the Ne atom influences the effective potential for the proton motion, resulting in a coupling between the intramolecular and intermolecular vibrations. The effect is expected to be most profound for the N–H stretch vibration. In order to account for the coupling, the N–H stretching vibrational energy levels ($v_1=0, 1$) were calculated with the Ne atom in different positions. The difference between the N–H vibrational energies for each vibrational state of the complex and the free monomer was then fitted to a functional form and added to the rigid monomer potential to produce effective intermolecular potentials for Ne-HN_2^+ without and with the N–H stretch excited. The method relies upon the adiabatic decoupling between the fast N–H stretch and the much slower intermolecular stretch and bend motions. Even for the ground vibrational state, due to zero point motion, the dissociation and rovibrational energies are significantly altered upon inclusion of the coupling.¹⁰

In more specific detail, the adiabatic correction function for the two-dimensional rigid monomer PES was constructed as follows. The N–H distance was varied for various positions of the Ne atom ($R=5.8, 6.3, 7.5 a_0$, $\Theta=0^\circ, 10^\circ, 20^\circ, 45^\circ, 60^\circ, 180^\circ$) to generate one-dimensional effective N–H stretch potentials. Subsequently, the vibrational energies of the N–H stretching vibrations were calculated using the LEVEL program³⁰ by approximating the ν_1 vibration as a pseudodiatom $\text{N}_2 \cdots \text{H}$ motion. While in the linear configuration ($\Theta=0^\circ$) strong shifts in the N–H vibrational frequency arise from the attraction between the proton and the neon atom, the vibrational energies for the antilinear ($\Theta=180^\circ$) orientation of the Ne atom are close to those of the free HN_2^+ ion.

The N–H vibrational band shifts for the $v_1=0$ and 1 levels were fitted to the following functional form to correct the rigid monomer PES:

$$V_{\text{corr}}(R, \Theta, v_1) = a_1(v_1) \exp[-a_2(v_1)R] \times \exp[-a_3(v_1) \exp\{-a_4(v_1)R\} \Theta^2]. \quad (1)$$

The fitting parameters $a_i(v_1)$ are listed in Table II. The vibrationally corrected surfaces are described by $V_0(R, \Theta) = V(R, \Theta) + V_{\text{corr}}(R, \Theta, v_1=0)$ and $V_1(R, \Theta) = V(R, \Theta) + V_{\text{corr}}(R, \Theta, v_1=1)$, where $V(R, \Theta)$ is the rigid monomer PES. The data for these three PESs can be obtained from Ref. 31. Figure 2 shows the ground state potential $V_0(R, \Theta)$ in more detail, while all three PESs V , V_0 , and V_1 are compared for $\Theta=0^\circ$ in Fig. 3 (with the relevant parameters given in Table III). The effect of correcting the rigid monomer PES is clearly visible even for Ne interacting with HN_2^+

TABLE III. Properties of the three PESs along with results of the rovibrational calculations. $\langle R \rangle$ and $\langle \Theta \rangle$ correspond to $\langle 1/R^2 \rangle^{-1/2}$ and $\arccos(\langle \cos^2 \Theta \rangle^{1/2})$. Experimental data are given in italics. For $v_1=1$, the values were not corrected for the Fermi resonance (see text).

	$v_1=0$ uncorrected (V)			$v_1=0$ corrected (V_0)			$v_1=1$ corrected (V_1)		
D_e (cm ⁻¹)	896			996			1255		
D_0 (cm ⁻¹)	711			795			1005		
R_e (Å)	3.288			3.260			3.209		
$\Delta\nu_1$ (cm ⁻¹)							210		
Expt							180.5		
	E (cm ⁻¹)	$\langle R \rangle$ (Å)	$\langle \Theta \rangle$	E (cm ⁻¹)	$\langle R \rangle$ (Å)	$\langle \Theta \rangle$	E (cm ⁻¹)	$\langle R \rangle$ (Å)	$\langle \Theta \rangle$
$\nu_s = \nu_b = 0$	0	3.321	7.21	0	3.295	6.84	0	3.235	6.1
Expt					3.281			3.246	
$\nu_s = 1$	120	3.366	7.45	128	3.338	7.06	148	3.276	6.3
Expt				138 ^a			158	3.297	
$\nu_b = 1$	104	3.325	12.9	117	3.302	12.2	146	3.247	10.6
Expt				98 ^a			128	3.247	

^aTentative assignment.

in its ground vibrational state, with an increase in the well depth (D_e) and curvature of the potential near the minimum and a decrease in the intermolecular bond length (R_e). The effects are even more pronounced in the $v_1=1$ state.

D. Rovibrational calculations

The PESs were used in rovibrational calculations to determine the intermolecular stretching and bending frequencies. The energies and wave functions were obtained using the Hamiltonian³²

$$\hat{H} = \hat{H}_{\text{mon}} - \frac{\hbar^2}{2\mu R} \frac{\partial^2}{\partial R^2} R + \frac{\hbar^2}{2\mu R^2} (\hat{J} - \hat{j})^2 + B_{\text{mon}}^{v_1} \hat{j}^2 + \hat{V}(R, \Theta, v_1). \quad (2)$$

Here \hat{J} is the angular momentum operator for the overall rotation of the complex, and \hat{j} signifies the internal angular momentum of the HN_2^+ moiety. The Hamiltonian was solved using the collocation method³² with the total wave function being expanded in a parity adapted basis set consisting of 22 radial and 25 angular Legendre polynomials. The lowest eigenvalues were converged to better than 0.5 cm⁻¹. The resulting properties for all three surfaces are compiled in Table III where they are compared to available experimental data.

The corrected PES for the $v_1=0$ state is characterized by a radial separation $R_e^{(0)} = 3.260$ Å and a well depth $D_e^{(0)} = 996$ cm⁻¹ (bracketed superscripts indicate the number of quanta in the intramolecular N–H stretch), with the dissociation energy (D_0) being 84 cm⁻¹ larger than for the rigid monomer PES. Accordingly, the intermolecular frequencies, $\nu_s^{(0)} = 128$ cm⁻¹ and $\nu_b^{(0)} = 117$ cm⁻¹, are higher than the ones calculated for the uncorrected PES. The averaged center of mass displacement in the vibrational ground state ($\langle 1/R^2 \rangle^{-1/2}$) is calculated to be 3.295 Å compared to 3.281 Å derived from the ground state rotational constant.

The corrected surface correlating with HN_2^+ in its $v_1=1$ state displays an increased well depth [$D_e^{(1)} = 1255$ cm⁻¹] and decreased equilibrium bond length [$R_e^{(1)}$

$= 3.209$ Å] compared to the ground state surface. The enhanced intermolecular interaction in the $v_1=1$ state is also reflected in increased intermolecular bending and stretching frequencies (Table III). The red shift for ν_1 , calculated as the difference between the D_0 values for Ne interacting with HN_2^+ in the $v_1=1$ and $v_1=0$ vibrational levels, is $\Delta\nu_1 = 210$ cm⁻¹ overestimating the experimental value by 30 cm⁻¹. The averaged center of mass displacement is calculated to be 3.235 Å which is slightly shorter than the experimental value of 3.246 Å.

There are two deficiencies in the adiabatically corrected PES. First, the MP2 level of theory is expected to take only part of the dispersion interaction into account. While working with larger basis sets at the MP4 level of theory may be preferable, the increase in computation time is considerable. Second, the adiabatic correction scheme adopted here only treats the N–H stretch coordinate, while coupling of the intramolecular bending and N–N stretch vibrations of the HN_2^+ core with the intermolecular motions are ignored.

IV. EXPERIMENTAL RESULTS AND DISCUSSION

A. Dimer

1. Spectra

From experience with the related complexes He-HCO^+ ,⁸ Ne-HCO^+ ,⁶ Ar-HCO^+ ,⁷ and He-HN_2^+ ,¹¹ it was expected that the mid-infrared spectrum of Ne-HN_2^+ should be dominated by a strong transition corresponding to excitation of the N–H stretching vibration of the complex (ν_1). In addition, a few weaker combination bands involving intermolecular vibrations were anticipated (e.g., $\nu_1 + \nu_b$, $\nu_1 + \nu_s$). Surprisingly, a somewhat more complicated spectrum was obtained. Figure 4 displays spectra of the normal and $\text{Ne-H}^{15}\text{N}_2^+$ isotopomers in the range of 2950–3150 cm⁻¹. The corresponding $^{22}\text{Ne-H}^{14}\text{N}_2^+$ spectrum is not shown, as it is, apart from a small red shift, very similar to the one of $^{20}\text{Ne-H}^{14}\text{N}_2^+$. For the normal isotopomer, five additional ro-

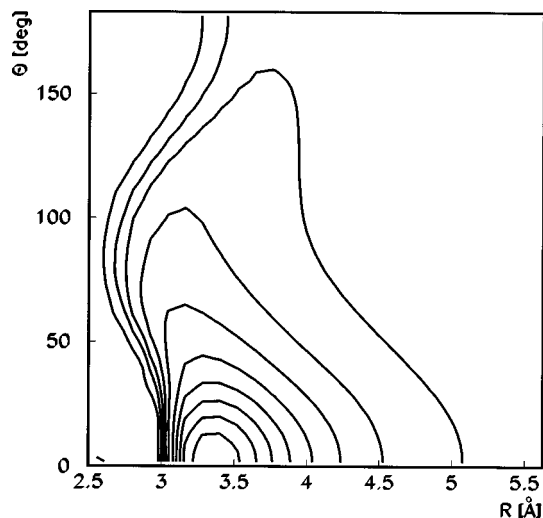


FIG. 2. Adiabatically corrected two-dimensional PES for ground state Ne-HN_2^+ , $V_0(R, \theta)$. The contours correspond to energies of 200, 0, -100, -200, -300, -400, -500, -600, -700, and -800 cm^{-1} , respectively.

tationally resolved bands were observed at higher frequencies (Fig. 5). A summary of the observed vibrational transitions for the Ne-HN_2^+ isotopomers in the 3000–3300 cm^{-1} region is presented in Fig. 6 in form of stick spectra. Rotational line wave numbers for the rotationally resolved bands for all isotopes are available from Ref. 31.

The spectra of Ne-HN_2^+ and $^{22}\text{Ne-HN}_2^+$ are dominated by two strong transitions with origins near 3054 and 3072 cm^{-1} , the former having roughly twice the intensity of the latter (Figs. 4 and 5). Below these two strong bands no photodissociation activity is detected down to 2700 cm^{-1} . The 3054 cm^{-1} transition is of the $\Sigma-\Sigma$ type with a characteristic $4B$ band gap and a prominent head in the P branch. The 3072 cm^{-1} transition also lacks Q branch lines but it is not clear whether it has a $4B$ band gap because of poor S/N in the gap region. The transition is virtually unshaded, although at $J \approx 40$ a weak head forms abruptly in the R branch (near 3081 cm^{-1}), apparently the result of a perturbation in the upper state.

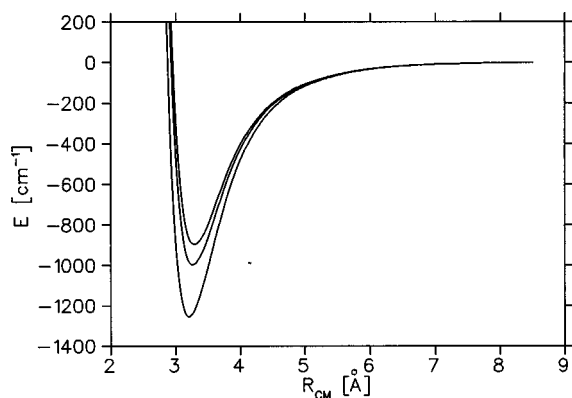


FIG. 3. Cuts through Ne-HN_2^+ PESs for the collinear configuration; rigid monomer PES (V , top) and the vibrationally corrected PESs for $v_1=0$ (V_0 , middle), and $v_1=1$ (V_1 , bottom). The adiabatic correction leads to an increased bond strength and a larger curvature of the potential near the minimum.

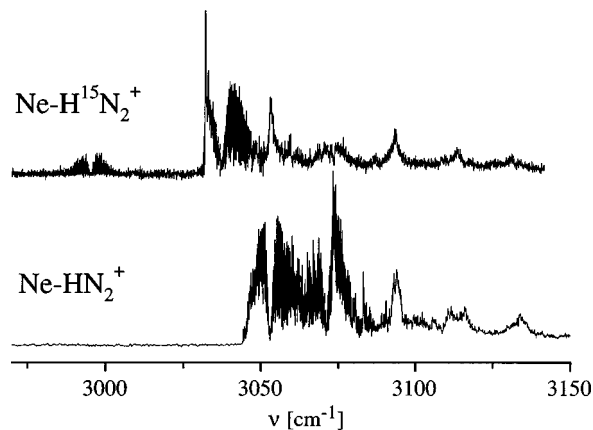


FIG. 4. Vibrational predissociation spectra of $^{20}\text{Ne-H}^{15}\text{N}_2^+$ (top) and $^{20}\text{Ne-H}^{14}\text{N}_2^+$ (bottom) in the region of the N–H stretching vibration.

Immediately to higher frequency a series of unresolved bands (denoted u_i) separated by roughly 20 cm^{-1} is observed, with the first and the most intense member lying under the R branch of the 3072 cm^{-1} transition. The separa-

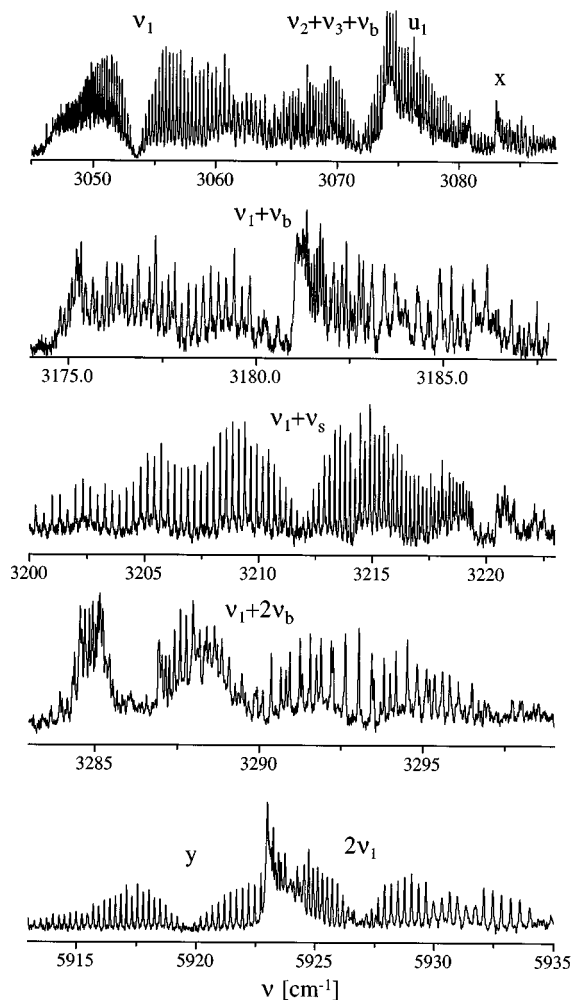


FIG. 5. Rotationally resolved transitions of $^{20}\text{Ne-H}^{14}\text{N}_2^+$ and their assignments. The bands x and u_1 are tentatively attributed to sequence transitions $\nu_1 + \nu_b - \nu_b$ and $\nu_1 + \nu_s - \nu_s$.

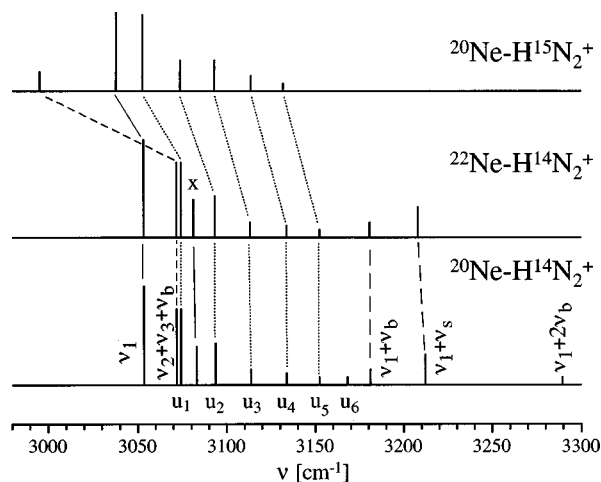


FIG. 6. Stick IR spectrum for the different Ne-HN_2^+ isotopomers, used to visualize frequency shifts and estimated relative band intensities. Transitions sharing the same assignments are interconnected. The bands x and u_i are tentatively attributed to sequence transitions.

tion between the first unresolved band and the 3054 cm^{-1} transition origin is of the same order of magnitude suggesting a certain interdependence. Six and five of these unresolved bands can be discerned in the spectra of Ne-HN_2^+ and $^{22}\text{Ne-HN}_2^+$, respectively. Their intensities decrease as they become separated from the 3054 cm^{-1} transition and their positions do not appear to be sensitive to $^{22}\text{Ne}/^{20}\text{Ne}$ isotopic substitution. The contours of these unresolved bands suggest that they may either contain Q branches or heads of highly degraded bands.

There are five more bands to higher energy (Fig. 5), including a weak perpendicular transition with a Q branch onset at 3181 cm^{-1} , a medium intensity $\Sigma-\Sigma$ band at 3212 cm^{-1} , a strongly perturbed parallel band at 3289 cm^{-1} , and two close lying $\Sigma-\Sigma$ bands, one at 5920 cm^{-1} and the other at 5927 cm^{-1} (all wave numbers refer to the normal isotopomer). The last three bands were only recorded for the normal isotopomer. For the perpendicular transition of $^{22}\text{Ne-HN}_2^+$ only the Q branch head position could be determined.

The spectrum of the $\text{Ne-H}^{15}\text{N}_2^+$ isotopomer is similar to the ones of $^{20}\text{Ne-HN}_2^+$ and $^{22}\text{Ne-HN}_2^+$ (Figs. 4 and 6). As expected, the overall spectrum shifts to lower frequencies because of the larger reduced mass for the intramolecular N-H vibration. Again, the spectrum contains two rotationally resolved parallel transitions and a group of near equidistant unresolved features. However, the relative intensities and separation of the two parallel bands differ from the other two isotopomers. The strongest band with origin at 3038 cm^{-1} is of the $\Sigma-\Sigma$ type and possesses a prominent head in the P branch, similar to the 3054 cm^{-1} transition of the normal isotopomer. Another weaker, rotationally resolved transition appears $\approx 42\text{ cm}^{-1}$ below the 3038 cm^{-1} band. The unresolved bands are separated from each other by roughly $18\text{--}21\text{ cm}^{-1}$ but only by 15 cm^{-1} from the 3038 cm^{-1} band. This is in contrast to the normal and ^{22}Ne isotopomers where the separation is around 20 cm^{-1} .

TABLE IV. Vibrational ground state molecular constants for the different Ne-HN_2^+ isotopomers determined from the fits of the averaged combination differences. Certain properties of the complex derived from the constants are also given.

	$^{20}\text{Ne-H}^{14}\text{N}_2^+$	$^{22}\text{Ne-H}^{14}\text{N}_2^+$	$^{20}\text{Ne-H}^{15}\text{N}_2^+$
B (cm^{-1})	0.121 94(2)	0.115 90(3)	0.118 14(10)
$D \times 10^{-7}$ (cm^{-1})	3.65(10)	3.26(10)	fixed at 3.50
ω_s (cm^{-1})	135(2)	133(2)	
k_s (N/m)	12.8(4)	13.0(4)	
$\langle R \rangle$ (\AA) ^a	3.281(1)	3.281(1)	3.371(2)
R_{NeH} (\AA) ^b	1.756(1)	1.756(1)	1.758(2)

^a $\langle R \rangle$ corresponds to $\langle 1/R^2 \rangle^{-1/2}$.

^b R_{NeH} was calculated using the B constant of the complex and the undistorted HN_2^+ structure taken from Ref. 44.

2. Ground state rotational constants

For the normal Ne-HN_2^+ isotopomer the lower state combination differences for all rotationally resolved bands agree to within experimental precision, suggesting that a common lower state is involved. It is believed that this is the ground state of the complex, as most of the ions are expected to be cooled in the expansion. In the case of $^{22}\text{Ne-HN}_2^+$ and $^{20}\text{Ne-}^{15}\text{HN}_2^+$, the lower state combination differences derived from the observed rotationally resolved transitions (3 for the former and 2 for the latter) also coincided. The lower state combination differences for the three isotopomers were weighted according to the band intensities, number of observed lines, and the accuracy of calibration, and then fitted to a standard linear molecule formula to give the ground state rotational constants provided in Table IV. This table also contains structural parameters for all three complexes derived under the assumption of the unchanged geometry of the HN_2^+ core, and estimations of the intermolecular stretching frequencies (ω_s) and force constant (k_s) from Millen's expressions.³³ Within experimental uncertainty the intermolecular bond distances and bond strengths are unaltered by isotopic substitution.

3. Vibrational assignments

The Ne-HN_2^+ vibrations can be partitioned into high frequency modes of the HN_2^+ core ($\nu_1 = \text{N-H stretch}$, $\nu_2 = \text{HNN bend}$, $\nu_3 = \text{N-N stretch}$) and low frequency intermolecular vibrations ($\nu_s = \text{intermolecular stretch}$, $\nu_b = \text{intermolecular bend}$). The assignment of rotationally resolved transitions is simplified by the fact that they all appear to originate from the ground state. Consequently, the respective transition origins in Table V provide direct access to the vibrational energies of the upper state levels.

As mentioned above, the ν_1 transition of the complex should be the strongest in the investigated range. Thus, the presence of two strong, parallel type bands at 3054 and 3072 cm^{-1} in the spectra of Ne-HN_2^+ and $^{22}\text{Ne-HN}_2^+$ is surprising, and indicates a strong interaction between ν_1 and another vibrational state, with the latter acquiring transition strength from the former. Because both bands display regular rotational line intensity distributions and an almost constant band-to-band intensity ratio for lines with the same upper J ($J=0\text{--}30$), it would appear that the two levels perturb each

TABLE V. Origins or peak maxima (in cm^{-1}) of the vibrational transitions observed in the spectra of different Ne–HN₂⁺ isotopomers. Bands x and u_i are tentatively assigned to sequence bands involving the intermolecular stretch and bend vibrations.

Band	²⁰ Ne–H ¹⁴ N ₂ ⁺	²² Ne–H ¹⁴ N ₂ ⁺	²⁰ Ne–H ¹⁵ N ₂ ⁺
ν_1	3053.54(2)	3053.26(2)	3037.85(2)
$\nu_2 + \nu_3 + \nu_b$ ($l=0$)	3071.85(2)	3071.70(2)	2995.37(2)
x^a	3083.05(3)	3081.10(2)	
$\nu_1 + \nu_b^a$	3181.04(5) ^b	3180.65(5)	
$\nu_1 + \nu_s$	3211.97(2)	3208.04(2)	
$\nu_1 + 2\nu_b$ ($l=0$)	3289.39(10)		
u_1	3074.3(3)	3074.2(3)	3052.6(3)
u_2	3093.7(4)	3093.4(3)	3073.9(1.0)
u_3	3113.7(3.0)	3113.1(3.0)	3093.0(6)
u_4	3133.7(6)	3133.8(6)	3113.7(6)
u_5	3152.3(1.2)	3152.4(1.2)	3131.9(1.2)
u_6	3168.1(1.2)		
y	5919.70(2)		
$2\nu_1$	5926.86(3)		

^a Q branch onset.

^bA value of 3181.17(2) cm^{-1} is obtained by fitting the P/R branch lines.

other by Fermi rather than a Coriolis interaction. In the case of a Coriolis interaction, the off-diagonal matrix elements are J dependent, so that the intensity ratio should vary with J , in contrast to observation.

Energies of vibrational levels of HN₂⁺ in the vicinity of ν_1 are gathered in Table VI. The lowest order intramolecular state in this region is $\nu_2 + \nu_3$ with an energy of 2947 cm^{-1} .³⁴ Could $\nu_2 + \nu_3$ be the interacting state? Apart from the fact that the symmetry species differs from ν_1 and the state would need to interact via a Coriolis coupling, the $\nu_2 + \nu_3$ level would appear to lie too low in energy. The energy of $\nu_2 + \nu_3$ in Ne–HN₂⁺ can be estimated from comparison with Ar–HCO⁺ for which a recent *ab initio* study predicted complexation induced frequency shifts of -270 , $+90$, and -30 cm^{-1} for ν_1 , ν_2 , and ν_3 respectively.²¹ For Ne–HN₂⁺, the Ne induced shift in ν_1 is around -170 cm^{-1} . If the solvent shifts for the three intramolecular vibrational frequencies scale similarly between Ar–HCO⁺ and Ne–HN₂⁺, the $\nu_2 + \nu_3$ level for Ne–HN₂⁺ should lie at approximately 2980 cm^{-1} , i.e., around 80 cm^{-1} below the 3054 and 3072 cm^{-1} bands. In fact, the predicted spacing between $\nu_2 + \nu_3$ and ν_1 for the Ne–HN₂⁺ complex lies close to the energy of the intermolecular bend vibration (ν_b). Thus, it may be the $l=0$ component of the $\nu_2 + \nu_3 + \nu_b$ state that is in Fermi resonance with ν_1 . Other assignments for the interacting state are less convincing. The $\nu_2 + \nu_3 + \nu_s$ combination

TABLE VI. Energies for selected vibrational states of HN₂⁺ (taken from Ref. 34).

Mode	Frequency (cm^{-1})
01 [±] 10	688
001	2258
04 ⁰ 0	2726
04 [±] 20	2749
04 [±] 40	2810
01 [±] 11	2947
100	3234

would necessarily interact with ν_1 via a Coriolis mechanism at variance with observation. The $l=0$ component of the 04⁰0 state lies too low in energy (2726 cm^{-1} , Table VI).

Examination of the spectrum of the Ne–H¹⁵N₂⁺ complex lends credence to the assignment of the two parallel bands as ν_1 and $\nu_2 + \nu_3 + \nu_b$. For the heavier isotopomer two close lying parallel type bands are observed at 3038 and 2995 cm^{-1} , with the latter being at least four times weaker than the former (Fig. 4). According to a theoretical CEPA-1 force field calculation, ¹⁴N/¹⁵N substitution in HN₂⁺ reduces ν_1 by only 19 cm^{-1} , while ν_3 is reduced by 66 cm^{-1} .³⁵ The bending vibration has not been considered in Ref. 35, however it should also decrease in frequency. Thus, the effect of ¹⁴N/¹⁵N substitution will be to move the ν_1 and $\nu_2 + \nu_3 + \nu_b$ bands further from resonance, resulting in reduced intensity for $\nu_2 + \nu_3 + \nu_b$, consistent with observation.

For the normal isotopomer, the intensity ratio of the ν_1 and $\nu_2 + \nu_3 + \nu_b$ bands of 2.0 ± 0.5 , together with the band separation of 18.3 cm^{-1} , allows one to conduct a simple deperturbation analysis.³⁶ Assuming that the intensity of both bands arises from their ν_1 component, one can estimate a 6 ± 2 cm^{-1} splitting between the two zero order levels and an interaction parameter of 8.5 ± 0.5 cm^{-1} . The more intense, lower-energy band is associated with a level having an eigenfunction $0.82|\nu_1\rangle + 0.57|\nu_2 + \nu_3 + \nu_b\rangle$ while the higher level is $0.57|\nu_1\rangle - 0.82|\nu_2 + \nu_3 + \nu_b\rangle$. The deperturbed frequencies are 3059.5 ± 1.0 and 3065.8 ± 1.0 cm^{-1} for ν_1 and $\nu_2 + \nu_3 + \nu_b$, respectively. For convenience, throughout the paper the two levels continue to be labeled by their dominant zero order component. At this stage, deperturbation of the ν_1 and $\nu_2 + \nu_3 + \nu_b$ bands in the Ne–H¹⁵N₂⁺ spectrum is difficult as the two bands were recorded in separate scans making relative intensities impossible to reliably estimate. However, assuming that the Fermi interaction parameter is insensitive to isotopic substitution, one can predict perturbation shifts of approximately 1.75 cm^{-1} for the ν_1 and $\nu_2 + \nu_3 + \nu_b$ levels of Ne–H¹⁵N₂⁺.

Rotationally resolved bands lying immediately to higher energy from the Fermi doublet are most likely due to combinations of ν_1 and the intermolecular modes. Intramolecular combination levels are sparse in this spectral range (Table VI) and moreover they are not expected to be strongly optically coupled with the ground state. For Ne–HN₂⁺, a weak perpendicular transition with a Q branch head at 3181 cm^{-1} , lying roughly 127.5 cm^{-1} above the ν_1 band, can be reliably assigned as the $\nu_1 + \nu_b$ combination, in accord with the rovibrational calculations on the adiabatically corrected $\nu_1 = 1$ PES (146 cm^{-1}). Consistent with this assignment is the transition's insensitivity to ²⁰Ne/²²Ne substitution. Nearby, at 3212 cm^{-1} is a $\Sigma-\Sigma$ type band which is shifted by ≈ 4 cm^{-1} towards lower energy for the ²²Ne isotopomer. The change in the rotational constant (ΔB) for this transition is negative indicating that the intermolecular bond is somewhat longer in the excited state than in the ground state. The isotopic shift and negative ΔB value encourage its assignment as the $\nu_1 + \nu_s$ combination. The excited state ν_s frequency is similar to the one in related proton bound complexes^{7,11} and agrees with the 148 cm^{-1} theoretical prediction. The assignment is also consistent with the shift in the bands' spacing

accompanying $^{20}\text{Ne}/^{22}\text{Ne}$ substitution. If the separation between the ν_1 and $\nu_1 + \nu_s$ bands (158 cm^{-1}) is inserted into a standard harmonic expression to estimate the frequency shift arising from the isotopic substitution, a value of 4.3 cm^{-1} is obtained in good agreement with observation. The $^{20}\text{Ne}/^{22}\text{Ne}$ substitution affects the frequency of the intermolecular stretch more than that of the bend. This is expected, as for the $\text{Ne}-\text{HN}_2^+$ rod-and-ball complex the reduced mass for the intermolecular stretch is more sensitive to the ball's mass than the intermolecular bend reduced mass.¹¹

Another weak parallel type transition is observed at 3289 cm^{-1} for the normal isotopomer. The position and structure of this band suggest its assignment to a transition into the Σ component of the $\nu_1 + 2\nu_b$ state. This band is separated from the $\nu_1 + \nu_b$ transition by roughly 108 cm^{-1} while the $\nu_1 + \nu_b$ to ν_1 separation amounts to 128 cm^{-1} .

The question arises as to why combination bands built on both ν_1 and $\nu_2 + \nu_3 + \nu_b$ are not observed in the spectrum. One reason for their absence may be that the frequencies of the intermolecular modes depend upon the vibrational state of the monomer. Thus, while ν_1 and $\nu_2 + \nu_3 + \nu_b$ lie close to one another, the spacing between combinations of type $\nu_1 + \nu_{s/b}$ and $\nu_2 + \nu_3 + \nu_b + \nu_{s/b}$ may be larger, reducing any Fermi interaction.

The transitions observed at 5920 and 5927 cm^{-1} (Fig. 5) are close to the expected position of $2\nu_1$. The $2\nu_1$ overtone has been observed for the HN_2^+ monomer at 6336.79 cm^{-1} and is predicted to have a transition strength 200 times less than the ν_1 fundamental.^{35,37} The presence of two transitions with comparable intensities in this region indicates that the $2\nu_1$ state of $\text{Ne}-\text{HN}_2^+$ is in Fermi resonance with a second vibrational level (denoted γ , Fig. 5). Candidates for the interacting level are numerous³⁴ and include $2\nu_2 + 2\nu_3$ and $\nu_1 + \nu_2 + \nu_3$ in combination with additional quanta of the intermolecular vibrations, making a positive assignment impossible at this stage.

Apart from the rotationally resolved bands, a series of unresolved features (u_i) is present in the spectra of all three isotopomers (Figs. 4 and 6). Their near-constant separation and decreasing intensity as the series progresses towards higher frequency, suggest that they may be hot bands. It is unlikely that ν_1 or ν_3 are involved since the sequence transitions for these two are shifted to lower frequencies with respect to the ν_1 band.³⁴ As well, complexes possessing quanta of ν_1 or ν_3 , or more than a single quantum of ν_2 would most probably dissociate before reaching the octopole region of the apparatus. To investigate whether complexes with internal energies exceeding the dissociation threshold survive the $50\text{--}100\ \mu\text{s}$ journey from the ion source to the octopole, spectra were recorded of $\text{Ne}-\text{HN}_2^+$ complexes that had been trapped in the octopole for several milliseconds. The relative intensities of all bands in the spectrum remained the same, indicating that if the unresolved bands are due to complexes with energies exceeding the dissociation threshold (e.g., with multiple quanta of ν_2) their predissociation lifetimes are exceedingly long ($>5\text{ ms}$).

Therefore it would appear that the unresolved bands are probably sequence bands of the type $\nu_1 + n\nu_b + m\nu_s - n\nu_b - m\nu_s$. According to the rovibrational calculations the ν_1

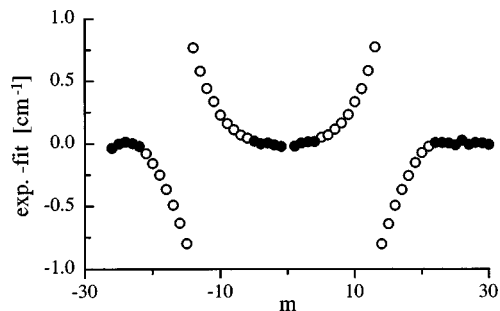


FIG. 7. Deviation between the experimental and fitted line positions for the $\nu_1 + 2\nu_b$ band of $^{20}\text{Ne}-\text{H}^{14}\text{N}_2^+$ at 3289 cm^{-1} showing the effect of a strong perturbation centered at $J' \approx 14$. In estimating the rotational constants of the upper state, only the transitions indicated by shaded circles were used.

$+ \nu_b - \nu_b$ and $\nu_1 + \nu_s - \nu_s$ transitions should be blue-shifted from ν_1 by 30 and 20 cm^{-1} , respectively. Assuming that the x and u_1 bands correspond to $\nu_1 + \nu_b - \nu_b$ and $\nu_1 + \nu_s - \nu_s$, the intermolecular frequencies for the $\nu_1 = 0$ state can be estimated as $\nu_b^{(0)} = 98\text{ cm}^{-1}$ and $\nu_s^{(0)} = 138\text{ cm}^{-1}$, the latter value being close to the harmonic stretching frequency of 135 cm^{-1} determined from the rotational constants (Table IV). A stiffening in the intermolecular stretching coordinate accompanying excitation of the N–H stretch is consistent with the theoretical predictions and also with observations for other similar complexes.^{6,8,9} As the combination bands $\nu_1 + \nu_b$ and $\nu_1 + \nu_s$ are resolved, one might expect that the sequence bands $\nu_1 + \nu_b - \nu_b$ and $\nu_1 + \nu_s - \nu_s$ should also display rotational structure. Indeed, numerous unassigned rotational lines are present in the highly congested region $20\text{--}30\text{ cm}^{-1}$ above ν_1 indicative of overlapping transitions.

The vibrational assignments proposed in this section are summarized in Table V. Some of the labels (e.g., $\nu_1 + 2\nu_b$) should not be taken as final and may change when further spectroscopic information is gathered.

4. Upper state rotational constants and perturbations

Using the ground state rotational constants, upper state parameters were obtained for all rotationally resolved bands. The line positions of each transition were fitted to a standard pseudodiatomic equation to obtain ν , B' , and D' , with the lower state constants being fixed. The analysis is complicated somewhat by the fact that almost all of the upper levels accessed in the study suffer from isolated perturbations affecting the regularity in the rotational line spacing. As an example, Fig. 7 displays the results of fitting the $\nu_1 + 2\nu_b$ band.

Fits of reasonable quality were obtained for the ν_1 bands of all three isotopomers. Rotational constants were determined by fitting transitions that terminated in $J' \leq 30$ levels, as anomalous variations in rotational line positions were observed for larger J values. For the R branch, only transitions up to $J \approx 35$ have been tabulated as higher J lines are obscured by the $\nu_2 + \nu_3 + \nu_b$ P branch. Difficulties were also encountered in fitting the higher J lines of the $\nu_2 + \nu_3 + \nu_b$ band for the normal and ^{22}Ne isotopomers. In both cases, a head in the R branch at around $J \approx 40$ is observed (near 3081 cm^{-1} , Fig. 5), possibly resulting from a localized per-

TABLE VII. Upper state molecular constants (in cm^{-1}) for rotationally resolved Ne–HN₂⁺ transitions. Ground state constants were fixed to values obtained from the combination differences analysis (Table IV). The third column indicates the J' range used for the fits. The last columns provide the constants and the standard deviations of the fits.

Band	Species	J' range for fit	ν	B	D ($\times 10^{+7}$)	σ ($\times 10^{+3}$)
ν_1	normal	$J' \leq 30$	3053.537(3)	0.124 28(2)	4.37(17)	4
	²² Ne	$J' \leq 30$	3053.264(2)	0.118 16(2)	4.1(2)	3
	¹⁵ N	$J' \leq 25$	3037.847(4)	0.120 84(3)	4.9(5)	4
$\nu_2 + \nu_3 + \nu_b$ ($l=0$)	normal	$J' \leq 20$	3071.850(2)	0.122 23(2)	6.0(6)	2
	²² Ne	$J' \leq 20$	3071.696(4)	0.116 04(5)	7.1(9)	5
	¹⁵ N	$J' \leq 25$	2995.369(6)	0.118 16(6)	4.5(9)	8
$\nu_1 + \nu_b$	normal	$P(30) - R(24)$	3181.171(5)	0.124 21(4)	4.5(4)	7
$\nu_1 + \nu_s$	normal	$J' \leq 25$	3211.971(3)	0.120 74(3)	4.1(3)	3
	²² Ne	$J' \leq 25$	3208.036(2)	0.114 76(3)	2.9(3)	3
$\nu_1 + 2\nu_b$ ($l=0$)	normal	$J' \leq 4$ and $J' = 22 - 29$	3289.34(2)	0.123 38(9)	16(1)	15
y	normal	$P(33) - R(15)$	5919.699(3)	0.122 65(2)	1.12(3)	6
$2\nu_1$	normal	$J' \leq 21$	5926.864(8)	0.125 44(6)	3.65 ^a	18

^aFixed at the ground state value.

turbation of the upper state rotational manifold. Lines with $J' \geq 40$ could not be identified in either the R or P branches. Thus, only a limited set of data ($J' \leq 20$ for ²⁰Ne–H¹⁴N₂⁺ and ²²Ne–H¹⁴N₂⁺, and $J' \leq 25$ for ²⁰Ne–H¹⁵N₂⁺) is fitted to obtain $\nu_2 + \nu_3 + \nu_b$ rotational constants and band origins.

Perturbations of the ν_1 and $\nu_2 + \nu_3 + \nu_b$ levels for $J > 30$ may arise through interaction with a third dark state, one likely candidate being the $\nu_2 + \nu_3 + \nu_s$ combination. While for low J this state should lie higher in energy than $\nu_2 + \nu_3 + \nu_b$, its B rotational constant should be smaller than for the other two levels, due to a lengthening of the intermolecular bond in the excited stretching state, and thus, at higher J the three states may approach one another producing the observed perturbations through a Coriolis interaction.

The upper state accessed in the $\nu_1 + \nu_s$ transition is also perturbed at around $J' = 40$. Hence, only lines up to $J' = 25$ were used for the fit. On the other hand, the $\nu_1 + \nu_b$ transition has unperturbed P and R branches. Its Q branch is not sufficiently well resolved to warrant analysis. For the $\nu_1 + 2\nu_b$ transition there is a strong perturbation located at $J' = 14$ (see Fig. 7), therefore transitions terminating in $J' = 5 - 21$ were excluded from the fit. The upper state rotational constants for all rotationally resolved bands are gathered in Table VII. The ΔB and D values for the rotationally resolved bands are in accord with the vibrational assignments proposed in the preceding section.

5. Discussion

The combined spectroscopic and computational studies provide detailed information on the structure and energetics of the Ne–HN₂⁺ complex. Intermolecular bond lengths can be determined from rotational constants, and conclusions concerning the flexibility of the intermolecular bond can be drawn from the frequencies of the intermolecular vibrations and from the centrifugal distortion constants.

The intermolecular frequencies for the $\nu_1=0$ and $\nu_1=1$ states are compared with the theoretical predictions in Table III. While there is reasonable agreement between theory and experiment for the frequencies of the intermolecular stretching vibrations, calculations using the corrected PESs overestimate the bending frequencies and the ν_1 red

shift somewhat. Similar differences between calculated and measured values have been previously observed for He–HN₂⁺.¹⁰ For He–HN₂⁺ and Ne–HN₂⁺ the calculated intermolecular bending frequency [$\nu_b^{(1)}$] is larger than the measured value by 18% and 12%, respectively. The calculated vibrational ν_1 red shifts for He–HN₂⁺,¹¹ Ar–HCO⁺,⁷ and Ne–HN₂⁺ also exceed the experimental values (by 17 cm^{-1} ,¹⁰ 47 cm^{-1} , and 30 cm^{-1} , respectively).

Despite the discrepancies, the theoretically determined PESs successfully predict the main characteristics of Ne–HN₂⁺, proving that the adiabatic correction procedure is suitable for near quantitative characterization of the ground and vibrationally excited states in such complexes. The principal advantage of the adiabatically corrected *ab initio* surfaces is that their calculation requires substantially less computational effort than a complete PES. Experimental and theoretical values for the intermolecular frequencies and the ν_1 red shift may eventually be brought into better agreement with a model that includes coupling of the monomer ν_2 and ν_3 vibrations with the intermolecular degrees of freedom.

An interesting result of the present work is the observation of the $2\nu_1$ level of Ne–HN₂⁺. This appears to be the first occasion on which an intramolecular overtone band of an ionic complex has been recorded with rotational resolution. The rovibrational data should eventually facilitate the development of an accurate potential energy surface that includes intramolecular and intermolecular coordinates, as has been accomplished for the Ar–HF complex.^{38–41} Neglecting the effect of Fermi resonances, the complexation induced red shifts for the ν_1 and $2\nu_1$ levels are 180 cm^{-1} and 410 cm^{-1} , respectively. The somewhat larger than linear dependence of the shift on the number of ν_1 quanta indicates that the Ne atom substantially influences the anharmonicity of the ν_1 vibration and emphasizes the strong interaction between the proton and the linearly disposed Ne atom. The increasing attraction between the Ne atom and the HN₂⁺ core as quanta are added to ν_1 is reflected in the marked decrease of the average intermolecular bond length with $\langle 1/R^2 \rangle^{-1/2} = 3.281$, 3.246, and 3.228 Å for $\nu_1 = 0, 1$, and 2.

It is interesting to compare the properties of Ne–HN₂⁺ and He–HN₂⁺ as both clusters have been investigated by

similar experimental and theoretical methods.^{10,11} For the most part, the effects of replacing He by Ne can be understood as resulting from an increase in the induction interaction, with a twofold increase in the polarizability of the rare gas. The enhanced rigidity and stability of Ne–HN₂⁺ is reflected in the increased intermolecular stretching force constant [$k_s^{(0)} = 12.8$ vs 4.8 N/m as estimated from the rotational and centrifugal distortion constants], and an increased well depth [$D_e^{(0)} = 996$ vs 542 cm⁻¹]. The intermolecular bending force constant also increases (by a factor of 3.2) when going from He–HN₂⁺ to Ne–HN₂⁺ (for complexes where ν_1 is excited). The intermolecular center of mass separations in both complexes are comparable ($(1/R^2)^{-1/2} = 3.295$ vs 3.276 Å).

The properties of Ne–HN₂⁺ can also be compared with those of the isoelectronic Ne–HCO⁺ complex.⁶ The proton affinity of CO (594 kJ/mol) exceeds that of N₂ (495 kJ/mol),³ so that one might anticipate a weaker interaction between the protonated end of the ion core and the Ne atom for HCO⁺ than for HN₂⁺. Indeed, this proves to be the case with the Ne–HCO⁺ and Ne–HN₂⁺ complexes having well depths of 483 and 996 cm⁻¹, intermolecular center of mass separations of 3.654 and 3.281 Å, and intermolecular stretching force constants of 4.8 and 12.8 N/m. As well, the red shift in the ν_1 vibration is also considerably smaller in Ne–HCO⁺ (42.5 vs 180.5 cm⁻¹).

Perturbations appear to be a common feature of the spectra of Rg–HCO⁺ and Rg–HN₂⁺ complexes (Rg=He, Ne, Ar), a situation most likely due to the fact that dissociation energies for the complexes are comparatively large and intermolecular vibrational frequencies are relatively low. Thus, any singly excited intramolecular vibration or simple combination state (e.g., ν_1 , $\nu_1 + \nu_s$) is likely to be nearby to at least one quasibound state involving multiple quanta of the intermolecular vibrations (e.g., $\nu_2 + n\nu_s + m\nu_b$, $\nu_3 + n\nu_s + m\nu_b$, $\nu_2 + \nu_3 + n\nu_s + m\nu_b$). The strength, variety, and number of perturbations is largest for the Ar–HCO⁺ and Ar–HN₂⁺ complexes, as these systems have relatively large dissociation energies and yet low vibrational frequencies (due to the heavy Ar atom).

The experimental results allow the predissociation lifetime of Ne–HN₂⁺ to be estimated. Given that dissociation ensues on time scales that are less than the ions' flight time through the octopole and that the linewidths for all rotationally resolved bands are laser limited (< 0.02 cm⁻¹), one can bracket the predissociation lifetime, 250 ps $< \tau_{vp} < 20$ μs.

B. Larger complexes

The mass selective nature of the experiment makes it feasible to investigate solvation effects in larger Ne_{*n*}–HN₂⁺ clusters. Figure 8 displays spectra of ²⁰Ne_{*n*}–¹⁴N₂⁺ ($n \leq 5$) clusters in the vicinity of the N–H stretching vibration obtained by detecting H¹⁴N₂⁺ ($n \leq 5$ clusters photofragment exclusively into HN₂⁺). The positions of the absorption maxima for each of the clusters are given in Table VIII. The ν_1 transition of the Ne–HN₂⁺ dimer is associated with a large red shift (180.5 cm⁻¹) from the free monomer value, whereas for the larger complexes smaller incremental shifts, $\Delta\nu_{\text{inc}}(n) = \nu_1(n) - \nu_1(n-1)$, back to higher frequencies are observed. As the cluster size increases, the incremental shifts

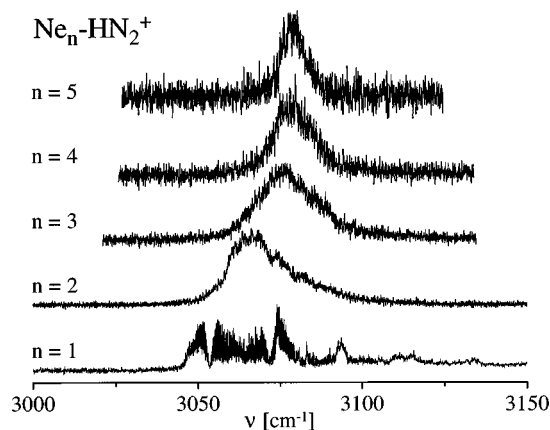


FIG. 8. Mid-infrared vibrational predissociation spectra of ²⁰Ne_{*n*}–H¹⁴N₂⁺ clusters in the region of the ν_1 stretching vibration of HN₂⁺.

become smaller, with virtually no difference between the positions of the ν_1 maximum for $n=4$ and $n=5$. The widths of the absorption features diminish with cluster size, possibly because of the smaller rotational constants and/or the destruction of the $\nu_1/\nu_2 + \nu_3 + \nu_b$ resonance.

Substantial but fruitless efforts were made to discern rotational structure in the Ne₂–HN₂⁺ spectrum. It is possible that the rotational features, which were anticipated to be apparent with the 0.02 cm⁻¹ bandwidth light source, are obscured by inhomogeneous broadening arising from the overlap of a number of hot bands or that rapid vibrational predissociation in the ν_1 state results in homogeneous line broadening. The lack of rotational structure in the ν_1 band parallels the situation for similar trimers [Ar₂–HCO⁺,⁷ Ne₂–HCO⁺,⁶ and He₂–HN₂⁺ (Ref. 11)].

Although the spectra of Ne₂–HN₂⁺ clusters with $n > 1$ do not display resolved rotational features, certain structural conclusions can be drawn from the evolution of the ν_1 band shifts with increasing cluster size, with the assumption that similar incremental shifts in ν_1 result from the addition of ligands to equivalent structural sites with respect to the central ion. For the Ne_{*n*}–HN₂⁺ complexes, the values of $\Delta\nu_{\text{inc}}(2)$ and $\Delta\nu_{\text{inc}}(3)$ are of similar magnitude (10–11 cm⁻¹) suggesting that the second and third Ne atoms occupy near equivalent positions with respect to the Ne–HN₂⁺ dimer core. However, the values for $\Delta\nu_{\text{inc}}(4)$ and $\Delta\nu_{\text{inc}}(5)$ are much smaller, of the order of 1–2 cm⁻¹, im-

TABLE VIII. Absorption maxima and widths of the ν_1 band in Ne_{*n*}–HN₂⁺ ($n=1-6$). All clusters dissociate into HN₂⁺.

<i>n</i>	Position (cm ⁻¹)	Width (cm ⁻¹)
1	3053.5 ^a	
2	3066 ± 3	20
3	3076 ± 3	20
4	3078 ± 2	14
5	3079 ± 2	9
6	≈ 3079 ^b	

^aNe–HN₂⁺ ν_1 origin.

^bEstimated value.

plying that sites further from the proton end of the molecule may be occupied by the fourth and fifth Ne atoms.

A similar approach was taken for the analysis of $\text{Ar}_n\text{-HCO}^+$ ($n=1-13$) spectra.⁷ In that case, the spectral shifts were interpreted in terms of geometries where a central Ar-HCO^+ core is progressively surrounded by two solvation rings each containing 4–5 Ar atoms, with the first solvation shell being completed by the twelfth Ar atom at the oxygen end of the core. Progressive addition of Ar atoms to the first solvation ring results in near constant displacements of the ν_1 band maximum ($\Delta\nu_{\text{inc}} \approx 25 \text{ cm}^{-1}$). At $n=6$ the solvation shift per added Ar atom becomes approximately 4 cm^{-1} , signaling the formation of the second solvation ring.

Although the qualitative trends observed in the spectra of $\text{Ne}_n\text{-HN}_2^+$ are the same as for the $\text{Ar}_n\text{-HCO}^+$ series, there are differences in the relative magnitudes of the incremental shifts of the ν_1 transition maximum ($\Delta\nu_{\text{inc}}$). For $\text{Ar}_n\text{-HCO}^+$, it was assumed that the total ν_1 frequency shift is dictated in first approximation by the interaction of the axial Ar atom with the central proton, and that the off-axial Ar atoms influence the total shift by weakening or strengthening this interaction. In this picture, Ar ligands from the second solvation ring that are further separated from the terminal Ar atom produce smaller incremental shifts in the ν_1 frequency than do ligands in the first ring. Applying this view to the $\text{Ne}_n\text{-HN}_2^+$ system, it appears that the fourth and the fifth Ne ligands may be nearer to the N end of Ne-HN_2^+ than the second and third ones suggesting that the development of the first solvation shell may be different in $\text{Ne}_n\text{-HN}_2^+$ and $\text{Ar}_n\text{-HCO}^+$.

The different rare gas ligand arrangements around HN_2^+ and HCO^+ may stem from their differing positive charge distributions. While in the former, the positive charge is shared almost equally between all three atoms,¹³ in the latter the charge is concentrated predominantly on carbon and to a lesser extent on hydrogen.^{42,43} As in a first approximation, the rare gas ligands arrange themselves so as to maximize the charge induced dipole interactions, in the small $\text{Ar}_n\text{-HCO}^+$ clusters a well defined ring of ligands is formed around the C–H bond. Here they influence the interaction between the terminal Ar atom and the proton, and produce a significant incremental blue shift in ν_1 . On the other hand, for HN_2^+ the sites along the entire HN_2^+ axis should be associated with similar binding energies. However, the Ne atoms bound to the N end of the core should have a minimal effect on the proton bound Ne atom and therefore on the ν_1 red shift.

A rough upper estimate for the average binding energies of the $n=2-6$ Ne ligands can be obtained by noting that a single IR photon with 3080 cm^{-1} energy is sufficient to fragment $\text{Ne}_6\text{-HN}_2^+$ into HN_2^+ and 6 Ne atoms. Neglecting the fragments' kinetic and internal energies, and assuming that Ne_n clusters are not formed in the fragmentation, one obtains an average binding energy for the $n=2-6$ Ne atoms as $(3080-795)/5=457 \text{ cm}^{-1}$ (795 cm^{-1} is the theoretical D_0 value of the terminal Ne atom). This implies a substantial disparity in the incremental binding energies of the first (terminal) Ne atom and subsequent ligands.

V. SUMMARY

Both the experimental data and the theoretical calculations indicate that Ne-HN_2^+ is a relatively rigid linear proton bound complex with a binding energy of 795 cm^{-1} and a Ne–H separation of the order of 1.76 \AA . The experimental values for the stretching and bending intermolecular vibrations of $^{20}\text{Ne-H}^{14}\text{N}_2^+$, observed in combination with ν_1 , are 158 and 128 cm^{-1} , respectively. The positions and rotational structures of most bands are affected by perturbations. Perhaps most significantly the ν_1 state appears to be in Fermi resonance with $\nu_2 + \nu_3 + \nu_b$ leading to the appearance of two strong bands in the 3000 cm^{-1} region. Most of the experimental observations can be reproduced by two-dimensional adiabatically corrected potential energy surfaces for Ne interacting with the HN_2^+ ion in its $v_1=0$ and $v_1=1$ states. While the spectra of larger complexes ($n \geq 2$) are not rotationally resolved, the size dependent positions of the ν_1 band can be explained in terms of cluster structures wherein the first Ne atom occupies the linear proton bound site and additional ones are weakly attached to the side of a Ne-HN_2^+ core.

ACKNOWLEDGMENT

This study is part of the project No. 20-49104.96 of the Swiss National Science Foundation.

- ¹P. B. Armentrout and T. Baer, *J. Phys. Chem.* **100**, 12866 (1996).
- ²D. Smith, *Chem. Rev.* **92**, 1473 (1992).
- ³S. G. Lias, J. E. Barmess, J. F. Liebman, J. L. Holmes, R. D. Levin, and W. G. Mallard, *J. Phys. Chem. Ref. Data Suppl.* **17**, 1 (1988).
- ⁴C. Lifshitz, in *Cluster Ions* (Wiley, New York, 1993), p. 121.
- ⁵S. A. Nizkorodov, Y. Spinelli, E. J. Bieske, J. P. Maier, and O. Dopfer, *Chem. Phys. Lett.* **265**, 303 (1997).
- ⁶S. A. Nizkorodov, O. Dopfer, M. Meuwly, J. P. Maier, and E. J. Bieske, *J. Chem. Phys.* **105**, 1770 (1996).
- ⁷S. A. Nizkorodov, O. Dopfer, T. Ruchti, M. Meuwly, J. P. Maier, and E. J. Bieske, *J. Phys. Chem.* **99**, 17118 (1995).
- ⁸S. A. Nizkorodov, J. P. Maier, and E. J. Bieske, *J. Chem. Phys.* **103**, 1297 (1995).
- ⁹S. A. Nizkorodov, J. P. Maier, and E. J. Bieske, *J. Chem. Phys.* **102**, 5570 (1995).
- ¹⁰M. Meuwly and R. J. Bemish, *J. Chem. Phys.* **106**, 8672 (1997).
- ¹¹M. Meuwly, S. A. Nizkorodov, J. P. Maier, and E. J. Bieske, *J. Chem. Phys.* **104**, 3876 (1996).
- ¹²E. J. Bieske, S. A. Nizkorodov, F. R. Bennett, and J. P. Maier, *J. Chem. Phys.* **102**, 5152 (1995).
- ¹³E. J. Bieske, S. A. Nizkorodov, F. Bennett, and J. P. Maier, *Int. J. Mass Spectrom. Ion Processes* **150**, 167 (1995).
- ¹⁴T. Speck, H. Linnartz, and J. P. Maier, *J. Chem. Phys.* **107**, 8706 (1997).
- ¹⁵R. V. Oikhov, S. A. Nizkorodov, and O. Dopfer, *J. Chem. Phys.* **107**, 8229 (1997).
- ¹⁶M. W. Crofton, J. M. Price, and Y. T. Lee, in *Clusters of Atoms and Molecules II* (Springer, Berlin, 1994), Vol. 56, p. 44.
- ¹⁷J. M. Lisy, in *Cluster Ions* (Wiley, New York, 1993), p. 217.
- ¹⁸E. J. Bieske and J. P. Maier, *Chem. Rev.* **93**, 2603 (1993).
- ¹⁹Y. Ohshima, Y. Sumiyoshi, and Y. Endo, *J. Chem. Phys.* **106**, 2977 (1997).
- ²⁰M. Kolbuszewski, *Chem. Phys. Lett.* **244**, 39 (1995).
- ²¹A. Nowek and J. Leszczynski, *J. Chem. Phys.* **105**, 6388 (1996).
- ²²D. Talbi and F. Pauzat, *Astron. Astrophys.* **229**, 253 (1990).
- ²³W. P. Kraemer, A. Komornicki, and D. A. Dixon, *Chem. Phys.* **105**, 87 (1986).
- ²⁴E. J. Bieske, *J. Chem. Soc., Faraday Trans.* **91**, 1 (1995).
- ²⁵G. Guelachvili and K. N. Rao, *Handbook of Infrared Standards* (Academic, London, 1993).
- ²⁶M. J. Frisch, G. W. Trucks, H. B. Schlegel, P. M. W. Gill, B. G. Johnson,

- M. A. Robb, J. R. Cheeseman, T. Keith, G. A. Petersson, J. J. A. Montgomery, K. Raghavachari, M. A. Al-Laham, V. G. Zakrzewski, J. V. Ortiz, J. B. Foresman, J. Cioslowski, B. B. Stefanov, A. Nanayakkara, M. Challacombe, C. Y. Peng, P. Y. Ayala, W. Chen, M. W. Wong, J. L. Andres, E. S. Replogle, R. Gomperts, R. L. Martin, D. J. Fox, J. S. Binkley, D. J. Defrees, J. Baker, J. P. Stewart, M. Head-Gordon, C. Gonzales, and J. A. Pople, Gaussian, Inc., Pittsburgh, Pennsylvania, 1995.
- ²⁷Extensible Computational Chemistry Environmental Basis Set Data Base, Version 10, 1996.
- ²⁸S. F. Boys and F. Bernardi, *Mol. Phys.* **19**, 553 (1970).
- ²⁹W. H. Press, S. A. Teukolsky, W. T. Vetterling, and B. P. Flannery, *Numerical Recipes in Fortran* (Cambridge University Press, Cambridge, 1986).
- ³⁰R. J. Le Roy, University of Waterloo Chemical Physics Report No. CP-330 LEVEL 5.0, University of Waterloo 1991.
- ³¹Data for the three potential energy surfaces and line positions of the rotational resolved bands of all isotopomers are available from the authors upon request.
- ³²A. C. Peet and W. Yang, *J. Chem. Phys.* **91**, 6598 (1989).
- ³³D. J. Millen, *Can. J. Chem.* **63**, 1477 (1985).
- ³⁴Y. Kabbadj, T. R. Huet, B. D. Rehfuss, C. M. Gabrys, and T. Oka, *J. Mol. Spectrosc.* **163**, 180 (1994).
- ³⁵P. Botschwina, *Chem. Phys. Lett.* **107**, 535 (1984).
- ³⁶C. H. Townes and A. L. Schawlow, *Microwave Spectroscopy* (Dover, New York, 1975).
- ³⁷H. Sasada and T. Amano, *J. Chem. Phys.* **92**, 2248 (1990).
- ³⁸H. C. Chang and W. Klemperer, *J. Chem. Phys.* **98**, 2497 (1993).
- ³⁹H. C. Chang, F. M. Tao, W. Klemperer, C. Healey, and J. M. Hutson, *J. Chem. Phys.* **99**, 9337 (1993).
- ⁴⁰J. T. Farrell, O. Sneh, A. McIlroy, A. E. W. Knight, and D. J. Nesbitt, *J. Chem. Phys.* **97**, 7967 (1992).
- ⁴¹J. M. Hutson, *J. Chem. Phys.* **96**, 6752 (1992).
- ⁴²B. Weis and K. Yamashita, *J. Chem. Phys.* **99**, 9512 (1993).
- ⁴³Y. Yamaguchi, C. A. Richards, and H. F. Schaefer III, *J. Chem. Phys.* **101**, 8945 (1994).
- ⁴⁴J. C. Owruksy, C. S. Gudeman, C. C. Martner, L. M. Tack, N. H. Rosenbaum, and R. J. Saykally, *J. Chem. Phys.* **84**, 605 (1986).